

# Electrochemically Mediated Direct CO<sub>2</sub> Capture by a Stackable Bipolar Cell

Ali Hemmatifar,<sup>[a]</sup> Jin Soo Kang,<sup>[a]</sup> Nil Ozbek,<sup>[a]</sup> Kai-Jher Tan,<sup>[a]</sup> and T. Alan Hatton<sup>\*[a]</sup>

The unprecedented increase in atmospheric CO<sub>2</sub> concentration calls for effective carbon capture technologies. With distributed sources contributing to about half of the overall emission, CO<sub>2</sub> capture from the atmosphere [direct air capture, (DAC)] is more relevant than ever. Herein, an electrochemically mediated DAC system is reported which utilizes affinity of redox-active quinone moieties towards CO<sub>2</sub> molecules, and unlike incumbent chemisorption technologies which require temperature or pH swing, relies solely on the electrochemical voltage for CO<sub>2</sub> capture and release. The design and operation of a DAC system is demonstrated with stackable bipolar cells using quinone chemistry. Specifically, poly(vinylanthraquinone) (PVAQ) nega-

tive electrode undergoes a two-electron reduction reaction and reversibly complexes with CO<sub>2</sub>, leading to CO<sub>2</sub> sequestration from the feed stream. The subsequent PVAQ oxidation, conversely, results in release of CO<sub>2</sub>. The performance of both small- and meso-scale cells for DAC are evaluated with feed CO<sub>2</sub> concentrations as low as 400 ppm (0.04%), and energy consumption is demonstrated as low as 113 kJ per mole of CO<sub>2</sub> captured. Notably, the bipolar cell construct is modular and expandable, equally suitable for small and large plants. Moving forward, this work presents a viable and highly customizable electrochemical method for DAC.

## Introduction


The unprecedented increase in the atmospheric concentration of greenhouse gasses (specifically CO<sub>2</sub>) with its direct effect on global climate patterns is of major concern for the 21st century. Atmospheric CO<sub>2</sub> levels which remained constant at around 280 ppm in the preindustrial era, have grown over recent decades to exceed 400 ppm, and the trajectory of ever-increasing anthropogenic CO<sub>2</sub> emissions suggests that the CO<sub>2</sub> level could be nearly doubled within this century.<sup>[1,2]</sup> The upper boundary of CO<sub>2</sub> concentration to avoid catastrophic climate and environmental changes was estimated to be around 500 ppm by the Intergovernmental Panel on Climate Change,<sup>[3]</sup> and we are approaching this limit at an alarming rate. Therefore, a multitude of technologies have been developed in an effort to mitigate CO<sub>2</sub> emissions: from solvent scrubbing<sup>[4]</sup> and oxy-fuel combustion<sup>[5]</sup> to thermal<sup>[6,7]</sup> or electrochemical methods<sup>[8,9]</sup> for CO<sub>2</sub> capture from the point sources (such as power plants) that are mostly responsible for the rise of atmospheric CO<sub>2</sub> concentration.

A significant contribution (roughly half) to overall CO<sub>2</sub> emissions can be attributed to distributed sources, and thus

removal of existing CO<sub>2</sub> from air (often noted as direct air capture, or DAC) is also essential for ensuring the CO<sub>2</sub> levels do not go beyond the targeted range.<sup>[10]</sup> DAC is a potential solution for climate change mitigation, with a number of technologies moving towards commercialization. While the applicability of DAC still requires validation, recent techno-economic assessments suggest reduction in CO<sub>2</sub> capture costs when implemented on a large-scale.<sup>[11]</sup> As the CO<sub>2</sub> concentration in ambient air is extremely dilute, chemisorbents with stronger affinity for CO<sub>2</sub> than typical sorbents used for point-sources have been employed for selective capture via DAC.<sup>[10,12]</sup> For instance, alkaline hydroxides<sup>[13–15]</sup> or carbonates<sup>[16,17]</sup> that strongly bind to CO<sub>2</sub> enable removal of CO<sub>2</sub> in the form of carbonate or bicarbonate, respectively, which then can be decomposed in a subsequent step to give a pure CO<sub>2</sub> stream for sequestration and regenerate the sorbent for additional capture of CO<sub>2</sub>. However, in addition to many of these sorbents being highly basic,<sup>[10]</sup> the thermodynamic benefit of CO<sub>2</sub> capture from ambient air comes with an energy penalty in the regeneration step, and an energy-intensive temperature swing is often needed to turn carbonate back to CO<sub>2</sub>-capture sorbents,<sup>[10,15]</sup> though there have been reports on emerging techniques to regenerate the sorbents near room temperature.<sup>[18,19]</sup> Ionic liquids have also been considered as potential sorbents for CO<sub>2</sub> capture as they have capabilities to dissolve CO<sub>2</sub>.<sup>[20]</sup> Significant advances were made through the introduction of functional groups such as amines,<sup>[21,22]</sup> but low gravimetric capacities of ionic liquids originating from their large molecular weight are challenges to overcome.<sup>[23]</sup> Alternatively, amine-functionalized porous supports (e.g., zeolites, metal-organic frameworks, etc.) show promising performances in DAC, as CO<sub>2</sub> can be chemisorbed on amine groups immobilized over large surface areas.<sup>[24–26]</sup> This method is favorable as it requires less energy input for regeneration of sorbents relative to conventional

[a] Dr. A. Hemmatifar, Dr. J. S. Kang, Dr. N. Ozbek, Dr. K.-J. Tan, Prof. T. A. Hatton  
Department of Chemical Engineering  
Massachusetts Institute of Technology  
Cambridge, MA 02139 (USA)  
E-mail: tahatton@mit.edu

 Supporting information for this article is available on the WWW under <https://doi.org/10.1002/cssc.202102533>

 © 2022 The Authors. ChemSusChem published by Wiley-VCH GmbH. This is an open access article under the terms of the Creative Commons Attribution Non-Commercial NoDerivs License, which permits use and distribution in any medium, provided the original work is properly cited, the use is non-commercial and no modifications or adaptations are made.

amine scrubbing methods (due to the lack of water in the process), but rapid decrease of CO<sub>2</sub>-capture capacity in long-term operations is an issue to be addressed.<sup>[25,26]</sup>

In recent years, there have been various attempts to incorporate electrochemical methods in CO<sub>2</sub> capture process.<sup>[27]</sup> Notably, the electrochemical swing methods are distinct from other techniques that require thermal cycling in that they rely solely on the electronic and/or electrochemical behavior of the active materials. These methods typically function by application of voltage (and/or current) to an electrochemical cell with one or more anode-cathode pairs and subsequent CO<sub>2</sub> capture/release through pH modulation,<sup>[28]</sup> electric double layer formation,<sup>[29,39]</sup> or nucleophilicity modulation of capturing moieties.<sup>[31]</sup> Electrochemically-mediated bonding has particular potential for use in DAC, since chemisorption has been proposed to be a more suitable approach than physisorption for the selective and efficient removal of CO<sub>2</sub> under low concentrations as well as in the presence of other gases.<sup>[12,32–34]</sup>

In the current work, we focus on the latter technique, in which electrochemically tunable affinity of moieties (such as quinones) towards CO<sub>2</sub> molecules allows cyclic capture and release of CO<sub>2</sub>. Voskian and Hatton<sup>[31]</sup> recently demonstrated an effective electro-swing adsorption bed system exploiting the ability of quinones to capture CO<sub>2</sub> under reducing conditions, and then to release this gas upon oxidation. In their system, it was necessary to directly address each of the cells in a stack individually, which can add complexity to the construction and operation of the beds. We here build upon and expand this work in both system design and operation to demonstrate a capture system with stackable bipolar cells using quinone chemistry for DAC. Specifically, we develop and construct a modular, expandable, and easy-to-fabricate cell stack with bipolar electrodes and demonstrate its applicability in DAC with feed concentrations as low as 400 ppm (0.04%) and energy consumption as low as 113 kJ mol<sup>-1</sup>. Notably, our proposed bipolar stack design eliminates the need for external electric interconnects between adjacent cells and ensures simpler implementation. Moreover, compartments other than essential components such as electrodes, electrolyte, and gas diffusion layer could be removed from the inside of the stacked bipolar cell, leading to a substantial improvement in terms of efficient volume utilization (i.e., less space needed for the system setup).

As shown in Figure 1, we employ the intrinsic affinity of redox-active quinone moieties towards CO<sub>2</sub> (in liquid phase) and use their reversible complexation with CO<sub>2</sub> molecules to demonstrate successful CO<sub>2</sub> capture and release from the gas phase (feed stream) via quinone reduction and oxidation, respectively. Specifically, to this end, we use poly(vinylanthraquinone)-carbon nanotube (PVAQ-CNT) composite cathodes and poly(vinylferrocene)-CNT (PVFc-CNT) composite anodes. In short, upon reduction at the cathode, quinone moieties in PVAQ-CNT (which is immobilized on a conductive substrate and wetted with an ionic liquid electrolyte) undergo two-electron redox reaction and complex with dissolved CO<sub>2</sub> molecules. The subsequent CO<sub>2</sub> deficit in the electrolyte (liquid phase) is then replenished by diffusive transport of CO<sub>2</sub> through the gas-liquid interface (from the gas to the liquid phase) and

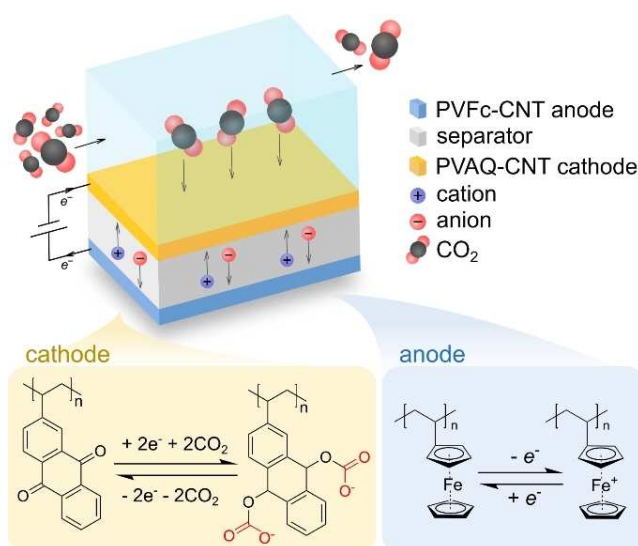


**Figure 1.** Schematic of the electrochemical cell with a PVAQ-CNT cathode and a PVFc-CNT anode for CO<sub>2</sub> separation from a feed stream. The anode and cathode composites are immobilized on a conductive substrate and are wetted with a room temperature ionic liquid. Cathode reduction results in quinone complexation with dissolved CO<sub>2</sub> and subsequent uptake of CO<sub>2</sub> from the feed stream. Cathode oxidation, on the other hand, results in decomplexation and release of CO<sub>2</sub>.

through the electrolyte from the interface to the quinone sites. Conversely, quinone oxidation results in decomplexation and diffusive release of CO<sub>2</sub> from the liquid towards the gas-liquid interface and finally into the gas phase (sweep stream).

We use a series of these capture modules to construct a novel, easy-to-fabricate, and highly modular bipolar stack (refer to Experimental Section for more information) and develop an integrated CO<sub>2</sub> capture/release system for DAC applications using computer-controlled valves and mass flow controllers (MFCs). We perform capture and release studies on a single-pair electrode cell (a proof-of-concept cell) as well as a meso-scale eight-pair bipolar cell, and demonstrate successful CO<sub>2</sub> uptake at concentrations as low as 400 ppm, which enables the operation at a narrower voltage window that leads to a small energy consumption. In short, our work lays out a viable electrochemical route for DAC based on the reversible carboxylation of quinone moieties using a modular and highly customizable bipolar cell.

## Experimental Section

### Materials

Reagents were purchased from Sigma Aldrich and PolySciences and used without further purification. The ionic liquid electrolyte obtained from IoLiTec Inc. was 1-butyl-3-methylimidazolium bis(trifluoromethylsulfonyl)imide ([BMIM][TFSI]). The electrode substrate was AvCarb EP40 carbon fiber paper without polytetrafluoroethylene (PTFE) treatment, obtained from Fuel Cell Store.

## PVAQ synthesis

PVAQ was synthesized via free-radical polymerization with slight modifications from a previously reported procedure.<sup>[35]</sup> 2-Vinyl-anthraquinone (2.13 mmol, 98%) and 2,2'-azobis(2-methylpropanitrile) (23  $\mu\text{mol}$ , 98%) were added to a three-necked flask, which was then vacuum purged with nitrogen. 1,2-Dichloroethane (21 mL, anhydrous 99.8%) was introduced into the vessel, and the dispersion was stirred and heated under reflux at 80 °C for 21.5 h. All components dissolved in the solvent upon heating, but the solution became cloudy again by the end of the reaction. The resulting mixture was allowed to cool to room temperature, after which the solid product was purified via multiple cycles of precipitation with methanol, separation by centrifugation, and re-dissolution in chloroform. The final washed polymer was dried under vacuum at room temperature with a yield of 82%.

## Electrode preparation and characterization

The electrodes in the flow cells used in this work were  $2 \times 2 \text{ cm}^2$ ,  $2.5 \times 15 \text{ cm}^2$ , and  $1 \times 15 \text{ cm}^2$  in size. The PVAQ-CNT and PVFc-CNT electrodes were both prepared by drop casting dispersion solutions onto the carbon paper substrates. A stock solution of 40 mg PVAQ and 120 mg multiwalled-CNT was dissolved in 20 mL N-methyl-2-pyrrolidone (NMP) solvent. Similarly, a second stock solution of 80 mg PVFc and 80 mg multiwalled-CNT dissolved in 20 mL NMP was also prepared. The polymers were dispersed with the CNTs via sonication of individual stock solutions for 1 h in an ice bath to generate separate PVAQ-CNT and PVFc-CNT inks. The inks were then drop cast onto their corresponding substrates in increments of 100  $\mu\text{L}$  and dried at 80 °C in a convection oven. Electrodes with various sizes and active material loadings were prepared during this work. Specifics of the size and loadings are given in the following sections accordingly. For the reference, 100  $\mu\text{L cm}^{-2}$  PVAQ-CNT loading is equivalent to 0.85  $\mu\text{mol PVAQ cm}^{-2}$  (or 0.8  $\text{mg cm}^{-2}$  of PVAQ-CNT), and 100  $\mu\text{L cm}^{-2}$  PVFc-CNT loading is equivalent to 1.87  $\mu\text{mol PVFc cm}^{-2}$  (or 0.8  $\text{mg cm}^{-2}$  of PVFc-CNT).

Further, electrochemical characterization (cyclic voltammetry, electrochemical impedance spectroscopy) and charge/discharge cycles (chronoamperometry and chronopotentiometry) were performed, respectively, on a PARSTAT 4000A potentiostat (Princeton Applied Research) and a Keithley 2440 sourcemeter (Keithley Instruments). Three-electrode characterizations were performed in a BASi cell with Pt wire and Ag/AgCl (3 M NaCl) counter and reference electrodes, respectively. Experiments were performed with [BMIM][TFSI] electrolyte under both  $\text{N}_2$  and  $\text{CO}_2$  (saturated) conditions.

## Stackable bipolar cell design

The bipolar cell, as shown in Figure 2, uses multiple capture modules with in-series electrical connections. Each module consists of a PVFc-CNT positive electrode, a separator, a PVAQ-CNT negative electrode, and a porous electrically conductive medium (such as titanium foam) serving as an air conduit. Specifically, as depicted in Figure 2a, each module was composed of (1) a pair of 185  $\mu\text{m}$  thick PVAQ-CNT and PVFc-CNT electrodes, (2) a 50  $\mu\text{m}$  thick polypropylene separator (Celgard), (3) a 1 mm thick nickel foam with 60 ppi pore size acting as air conduit, and (4) titanium sheets acting as current collectors. The modules were stacked face to face as in Figure 2b, resulting in a series of capture modules in which the opposite electrodes of adjacent modules are electrically – but not ionically – connected via the air conduit (hence the name bipolar stack), while opposite electrodes in the same module are ionically – but not electronically – connected by the separator. The assembly

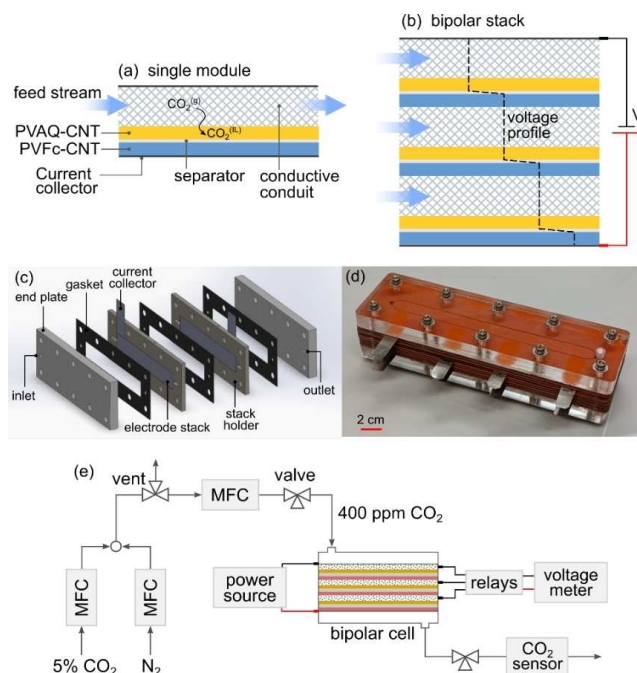


**Figure 2.** Schematic of (a) a single capture module and (b) a bipolar cell with multiple in-series modules (three pairs shown). (c) Simplified three-dimensional (3D) drawing and (d) photograph of the cell. Modules consist of anode, cathode, separator, and porous conductive air conduit. The stacking provides electrical contact between opposite electrodes of adjacent modules (via the conductive air conduit) and ionic connection between opposite electrodes in the same module (via the separator). By design, the external voltage is then simply equally split between the electrode pairs, driving similar capture dynamics in each module. (e) Schematic diagram of our continuous  $\text{CO}_2$  capture and release system with MFCs, three-way valves, power source,  $\text{CO}_2$  sensor, and our electrochemical cell. A power source was used for application of voltage/current to the cell. A digital multimeter with a custom-built eight-channel relay pack was used to monitor the voltage of individual modules.

was then sandwiched between two acrylic endplates and sealed with silicone rubber gaskets and fasteners (McMaster-Carr). We henceforth call this assembly the *stackable bipolar cell* (or simply, the *cell*). The design described here, which to some extent is reminiscent of the fuel cell structure, eliminates the need for external electric interconnects between the adjacent modules and ensures simpler implementation while greatly increasing the modularity. The external voltage is simply equally split between electrode pairs, driving the quinone redox reactions and subsequent capture and release of  $\text{CO}_2$ .

## Carbon capture and release platform

The capture and release platform, as shown in the schematic of Figure 2e, was composed of  $\text{N}_2$  and 5%  $\text{CO}_2$  (in nitrogen) feed gas lines (Airgas), three MFCs (Cole-Parmer), computer-controlled three-way valves, a power source, a flow-through  $\text{CO}_2$  sensor (ExplorIR-W 5%), and our bipolar cell. We note that the gas mixture of  $\text{N}_2$  and  $\text{CO}_2$  was used here for the cell operation due to the oxygen sensitivity of quinones. These experiments were designed specifically to demonstrate the operational behavior of the quinone-based electrochemical  $\text{CO}_2$  capture system in a stackable bipolar cell configuration, which would let us draw connection between the current finding and practical application (which uses the air as the feed stream) once the oxygen-sensitivity challenge is resolved. The

two feed streams were mixed at 125:1 ratio to generate a 400 ppm (0.04%) CO<sub>2</sub> stream in N<sub>2</sub> carrier gas with total flowrate of 600 mL min<sup>-1</sup>. This corresponds to flowrates of roughly 4.8 and 595.2 mL min<sup>-1</sup>, respectively, which are comfortably within the operating range of each MFC. The resulting 400 ppm CO<sub>2</sub> stream was then passed through a third MFC, reducing the flowrate to 5 mL min<sup>-1</sup> by venting the excess flow directly to the atmosphere; the use of only two MFCs (instead of three), resulted in an exceedingly slow and hard to achieve flowrate for the 5% CO<sub>2</sub> stream. The final 400 ppm feed stream was then passed through the bipolar cell, and, subsequently, the flow-through CO<sub>2</sub> detector. The two computer-controlled valves immediately upstream and downstream of the cell stack were used to allow or block the feed through the cell on demand. A power source (Keithley 2440) was used for application of voltage/current to the cell, and a single-channel digital multimeter (Fluke) in conjunction with a custom-built 8-channel relay pack was used to monitor the voltage level of individual modules during the operation of the cell. All components of the setup (MFCs, valves, power source, relays, voltage meter, and CO<sub>2</sub> sensor) were connected to and controlled by a computer.

## Results and Discussion

### Electrochemically mediated CO<sub>2</sub> separation

Quinone moieties, and thus PVAQ polymers, undergo two-electron charge transfer upon oxidation and reduction in aprotic electrolytes and can reversibly complex with electrophiles such as CO<sub>2</sub> (but not N<sub>2</sub>) during the process.<sup>[31,36,37]</sup> This reversible carboxylation of PVAQ-CNT electrodes results in great selectivity towards CO<sub>2</sub>, and, once paired with counter electrodes such as PVFc-CNT to balance the charge, can be a viable solution for carbon capture applications. Further, the electrolyte can play a significant role in the operation of the cell. Specifically, due to flow of gas over the wetted electrodes, electrolyte evaporation can be a major concern. Aqueous electrolytes require frequent electrolyte replenishment, and, moreover, tend to dissolve quinones, resulting in quick capacity fade. Room temperature ionic liquids (RTILs), however, have negligible vapor pressure with minimal evaporation and eliminate the need for electrolyte replenishment. In this work, [BMIM][TFSI] electrolyte is used due to its low vapor pressure and good CO<sub>2</sub> solubility (around 4 g L<sup>-1</sup>).<sup>[38]</sup>

Figure 3 shows cyclic voltammograms (CVs) of individual electrodes in a three-electrode setup (BASi) with Pt wire counter electrode and a leakless Ag/AgCl reference (eDAQ) in [BMIM][TFSI] electrolyte at a slow scan rate of 5 mV s<sup>-1</sup>. As evident from the CV curve, the PVAQ-CNT cathode in CO<sub>2</sub>-deprived electrolyte (under N<sub>2</sub> atmosphere) has two distinct reduction peaks corresponding to two-step activation of quinone centers in the absence of CO<sub>2</sub>. In a CO<sub>2</sub>-rich environment, on the other hand, the two peaks merge into a single peak close to the first reduction potential, which is a direct indication of reversible complexation of quinone centers with dissolved CO<sub>2</sub>, with a redox potential of around -0.7 V (measured as the average of reduction and oxidation potentials). Together with the PVFc-CNT electrode, the electrochemical voltage window (measured as the distance between

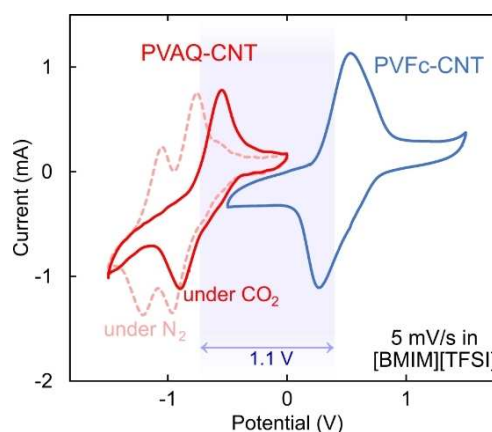


**Figure 3.** CVs of PVAQ-CNT and PVFc-CNT electrodes in three-electrode setup (Pt counter and Ag/AgCl reference electrode) in [BMIM][TFSI] electrolyte at 5 mV s<sup>-1</sup> scan rate. Notably, PVAQ-CNT shows two distinct quinone redox peaks in the absence of CO<sub>2</sub> (under N<sub>2</sub>), while the two peaks merge in a CO<sub>2</sub>-rich environment. In the cathodic scan, the second reduction peak (located at a more negative potential) undergoes positive potential shift by the complexation between quinone and dissolved CO<sub>2</sub>; formation of carbonate at one of the carbonyl groups makes the quinone aromatic ring relatively neutral, leading to a facilitated reduction of second carbonyl group that leads to nucleophilic addition of another CO<sub>2</sub> [forming quinone bis(carbonate)]. In the anodic scan, one peak appears under CO<sub>2</sub> at a relatively positive potential compared to those observed under N<sub>2</sub>. This is attributable to the larger driving force required for oxidation of quinone bis(carbonate) than that needed for quinone dianion oxidation.<sup>[37]</sup>

average redox potential of PVAQ-CNT and PVFc-CNT electrodes) is approximately 1.1 V. As a result, in a cell with a PVFc-CNT anode and a PVAQ-CNT cathode, one can expect complete activation of both quinone and ferrocene moieties theoretically at voltages above 1.1 V, although a larger voltage window would be needed to overcome the kinetic barriers.

### Capture and release cycles: proof of concept

Before study of a multi-pair electrode cell, in this section, we demonstrate capture and release cycles in a small-scale cell with a single electrode pair. The cell had a bed volume – the empty space within the cell through which the gas flow and contact occurs – of 1.5 mL with 2×2 cm<sup>2</sup> electrodes, and the feed stream was 400 ppm CO<sub>2</sub> in N<sub>2</sub> carrier gas. The electrode loadings were 0.3 μmol cm<sup>-2</sup> PVAQ-CNT and 0.6 μmol cm<sup>-2</sup> PVFc-CNT. In the following, we first demonstrate the capture and release of atmospheric-level CO<sub>2</sub> (400 ppm) in a three-step cycle (capture, release at no-flow, and flush) and later show continuous cyclic operation of the cell under quasi-steady-state condition.

Figure 4a shows effluent CO<sub>2</sub> concentration vs number of bed volumes (i.e., total volume gas introduced to the cell relative to the actual bed volume available for flow) for the cell operated in a capture-release-flush sequence. Prior to start of the experiment, a constant flow of N<sub>2</sub> at 5 mL min<sup>-1</sup> was fed to the cell for 1 h. The feed gas was then immediately switched to 400 ppm CO<sub>2</sub> (at *t* = 0) and a voltage of 1.5 V was applied

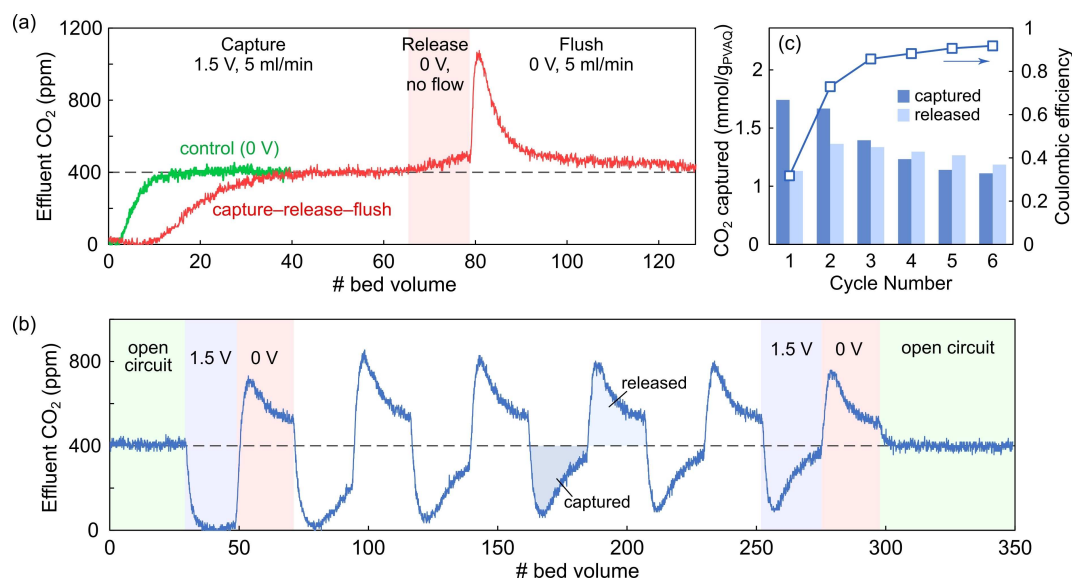


**Figure 4.** (a) Effluent CO<sub>2</sub> concentration vs bed volume for capture-release-flush cell operation as well as the control run. The breakthrough curves during the capture step show complete CO<sub>2</sub> removal of about 10 bed volumes with subsequent concentration recovery that is slower compared to the control experiment. (b) Cyclic operation of a fresh cell with 1.5 and 0 V during capture and release steps, respectively. Dynamic steady state is achieved after six cycles. (c) Captured and release amounts of CO<sub>2</sub> as well as Coulombic efficiency during each cycle.

across the cell. The capture-release-flush sequence is as follows: (1) capture step upon application of 1.5 V to the cell and under 5 mL min<sup>-1</sup> flowrate, (2) release step at 0 V cell voltage and stopped flow, and finally (3) flush step under the flow of 400 ppm CO<sub>2</sub> with 5 mL min<sup>-1</sup> flowrate at the same cell voltage (0 V). A separate control experiment under the same conditions but at 0 V throughout was also performed. The control is used to reveal the mixing and gas dispersion effects in the cell in the absence of electrochemical CO<sub>2</sub> uptake. As evident from Figure 4a, the breakthrough curve for the control experiment shows an initial region with zero effluent CO<sub>2</sub> concentration, followed by a sharp increase in the concentration. The two regions correspond respectively to (1) the delay due to gas detector position and (2) convective transport and dispersion of the gas inside the cell. The capture/release experiment shows a similar breakthrough profile, but with two important differences: complete CO<sub>2</sub> removal up to 10 bed volumes, and slower effluent concentration recovery compared to the control experiment. The latter is partly due to dispersion of gas and partly to electrochemical adsorption of CO<sub>2</sub> into the cell. The area between the two breakthrough curves is indicative of the amount of CO<sub>2</sub> captured, which is approximately equal to the released amount during the flush step, as expected.

Figure 4b shows cyclic operation of a fresh cell for six complete cycles at 1.5 and 0 V during the capture and release steps, respectively, each for a duration of around 800 s (45 bed volumes). The results show successful capture and release of CO<sub>2</sub> at the low concentration of 400 ppm, even in presence of N<sub>2</sub> gas in 2500-fold abundance. The cell achieves near-complete removal of CO<sub>2</sub> in the first cycle but only partial release at 0 V, with the captured amount being significantly larger than the released amount (refer to Figure 4c). While these effects are

partially due to mass transfer limitations within the electrolyte and across the gas-liquid interface, and have been attributed to a tradeoff between capacity and throughput of the system in other flow studies,<sup>[39,40]</sup> the primary reason is the physical solubility of CO<sub>2</sub> in the electrolyte in equilibrium with the sweep stream; when the electrodes are reactivated for adsorption, this residual CO<sub>2</sub> immediately complexes with the quinones, reducing their availability for capture of CO<sub>2</sub> from the fresh feed stream. A simple modeling analysis of these issues is given in a later section, where it is shown that the capacity is directly impacted by the amount of CO<sub>2</sub> captured by the activated quinones relative to that physically dissolved in the electrolyte. After a number of cycles, the cell reaches dynamic steady state in which subsequent cycles become progressively similar, as is evident from Figure 4c, where CO<sub>2</sub> uptake and released amounts converge. The amounts (in moles) are calculated by integrating the area bounded by the CO<sub>2</sub> concentration profile and 400 ppm line (inlet concentration) using the relation below:

$$N = \frac{Q}{RT} \int p_{\text{CO}_2} dt = \frac{V_{\text{bed}}}{RT} \int p_{\text{CO}_2} dn_{\text{bed}} \quad (1)$$

with  $Q$ ,  $V_{\text{bed}}$ ,  $R$ , and  $T$  being the flowrate, bed volume, universal gas constant, and temperature (20 °C), respectively,  $t$  and  $n_{\text{bed}}$  are time and number of bed volumes, and  $p_{\text{CO}_2}$  is CO<sub>2</sub> partial pressure in the feed stream which is related to the ppm value  $c_{\text{ppm}}$  as in  $p_{\text{CO}_2} = (10^{-6} c_{\text{ppm}}) p_{\text{atm}}$  with  $p_{\text{atm}}$  being the atmospheric pressure. Lastly, Figure 4c also shows the Coulombic efficiency of up to around 92% (defined as charge transferred during charging over that during discharging), suggesting effective direct air capture using quinone chemistry and the fabricated cell. The low efficiency in the first cycle is because a

part of the CO<sub>2</sub> released by the quinones remains physically in the electrolyte solution and does not transport to the sweep stream.

### Voltage distribution and capture dynamics

We here discuss the effectiveness of the bipolar stack in splitting the voltage equally across multiple electrode pairs and the associated mass transport limitations. Figure 5a and b show an example of cell and module voltages, current, and effluent concentration profiles for a bipolar cell with three electrode pairs (denoted as modules 1 to 3) with 400 ppm influent CO<sub>2</sub> and 5 mL min<sup>-1</sup> flowrate. The cell had active material loading density similar to that in the previous section, but with larger electrodes (2.5 × 15 cm) and bed volume (12 mL). The experiment consisted of a capture step at 3.6 V (1.2 V across each module) for a duration of 2 h, followed by a series of release and flush steps at 3, 2.4, 1.8, 1.2, 0.6, and 0 V levels. Release and flush steps were performed under no-flow and 5 mL min<sup>-1</sup> flowrate conditions, respectively. Results in Figure 5a, as expected, show equal voltage split across the three modules, with positive current during capture and negative current during subsequent release steps, confirming the effectiveness of our bipolar stack design. The results in Figure 5b show almost complete CO<sub>2</sub> removal during the capture step and step-wise release during the subsequent flush steps.

The capture dynamics during charging at 3.6 V are presented in Figure 5c, where we compare the cumulative captured amount (in μmol of CO<sub>2</sub>) and the theoretical value of complete CO<sub>2</sub> removal (dashed line). The captured amount  $N$  is

calculated as  $N = Q \int (c_{in} - c_{out}) dt$  with  $c_{in}$  and  $c_{out}$  being inlet and outlet CO<sub>2</sub> molar concentrations, respectively, where the molar concentration  $c$  is related to ppm value  $c_{ppm}$  as in  $c = \frac{p_{atm}}{RT} (10^{-6} c_{ppm})$ . The results show two distinct regions: (1) an initial advection-limited region up to about 30 bed volumes with complete CO<sub>2</sub> removal, followed by (2) a diffusion-limited region where capture rate progressively slows down, possibly due to mass transfer limitations within the electrolyte and/or across the gas-liquid interface as the electrolyte equilibrates with the gas stream. Lastly, Figure 5d summarizes the cumulative CO<sub>2</sub> amount released vs electrochemical voltage window of each module ( $\Delta V$ ), defined for our 3-pair electrode cell as  $\Delta V = \frac{1}{3}(3.6 - V_{release})$ . The data suggest a sigmoidal trend for release of CO<sub>2</sub> vs the module voltage window, where  $\Delta V < 0.7$  V results in less than 20% CO<sub>2</sub> release and  $\Delta V > 1.3$  V has diminishing effect on the released amount. This is in accordance with Nernst equation predictions with an around 1.1 V electrochemical voltage for the PVAQ-CNT / PVFc-CNT cell discussed earlier and suggests the optimized operation to be at (or slightly larger than) the electrode pair electrochemical voltage (e.g., 1.2 V). Voltage windows much wider than 1.3 V are not favorable, as they increase the energy consumption without appreciable increase in the system throughput. Additionally, as shown by Voskian and Hatton,<sup>[31]</sup> lower energetics can be attained with working capacities (i.e., released amount vs maximum capacity) of about 50%–60%, corresponding here to a cell voltage of about 0.8 V.

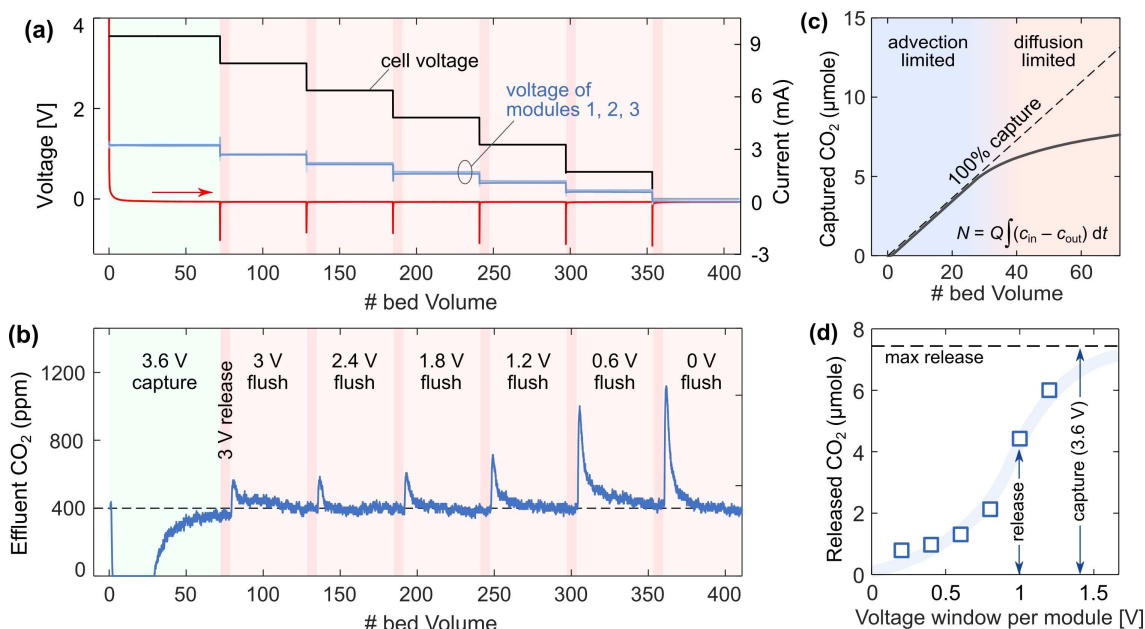


**Figure 5.** (a) Voltage of the cell and individual modules as well as the measured current and (b) effluent concentration during capture at 3.6 V and stepwise release and flush at 3, 2.4, 1.8, 1.2, 0.6, and 0 V. Results show near-perfect voltage split across the modules. (c) Cumulative captured amount vs bed volume reveals an initial advection-limited region followed by a diffusion-limited region. (d) Cumulative released CO<sub>2</sub> vs electrochemical voltage window of each module.

### Capture and release with bipolar stack

In this section, we discuss direct air capture (and release) and the associated energy consumption via the meso-scale eight-pair cell discussed in the Experimental Section. The cell had about 14 mL bed volume with  $1 \times 15 \text{ cm}^2$  electrodes with loadings of  $0.5 \mu\text{mol cm}^{-2}$  (PVFc-CNT) and  $0.25 \mu\text{mol cm}^{-2}$  (PVAQ-CNT), operating at a  $5 \text{ mL min}^{-1}$  flowrate. Importantly, inspired by the observations made in the previous section and in an attempt to minimize the overall energy consumption, we limit the operating voltage window of each module to between 1.2 V (for capture) to 0.6 V (for release) and thus operate the cell in 4.8 to 9.6 V range. Additionally, each capture and release cycle consisted of an initial constant current step ( $\pm 0.5 \text{ mA}$ ) followed by operation for a period with constant voltage across the cell. The current is limited to prevent excessive resistive (Coulombic) loss during the voltage switch. Figures 6a and b show voltages of individual modules, total current, and the effluent  $\text{CO}_2$  concentration for seven consecutive cycles. Results show roughly similar voltage profiles for the eight modules (0.6 to 1.2 V) in the bipolar stack. The narrower flow channel (compared to  $2.5 \times 15 \text{ cm}^2$  in the previous section) enabled a more efficient capture of  $\text{CO}_2$  as shown in Figure S1 (Supporting Information). Additionally, similar to Figure 4b, the effluent concentration profile reaches a dynamic steady state, resulting in stable capture and release after 6–7 cycles.

The corresponding specific energy consumption ( $\text{kJ mol}^{-1} \text{CO}_2$ ) shown in Figure 6c continuously decreases: from  $900 \text{ kJ mol}^{-1}$  in the first cycle down to around  $100 \text{ kJ mol}^{-1}$  during the steady state operation of the cell. The values here are calculated as the sum of electrical and pneumatic work over the course of a single cycle; we note, however, that the pressure drop across the cell at  $5 \text{ mL min}^{-1}$  flowrate is on the order of tens of Pa, resulting in negligible pneumatic energy consump-

tion. The trend in Figure 6c clearly shows a tradeoff between capture rate and energy efficiency: the first cycle demonstrates highest capture amount (and highest capture rate) at the expense of lowest energy efficiency ( $\approx 900 \text{ kJ mol}^{-1}$ ), while subsequent cycles with lower capture amount require progressively less energy down to only around  $100 \text{ kJ mol}^{-1}$ . This level of energy consumption matches that in the state-of-the-art DAC systems, with reported values in the range of  $100\text{--}150 \text{ kJ mol}^{-1}$ . That said, we note that the interplay of the two metrics together, and not just the energy consumption, defines the figures of merit relevant to practical DAC operation and plant design. We note below that the physical solubility of the  $\text{CO}_2$  in the electrolyte plays an important role in dictating the overall performance of the system for any given quinone loading.

### Notes on operation of a full-size system

In this work, we focused on capture of  $\text{CO}_2$  from a feed with release to a sweep stream at the same  $\text{CO}_2$  partial pressure  $p$  (corresponding to a concentration of 400 ppm) to demonstrate the cyclic operation under flow conditions. In practice, however, it would be desirable to recover the  $\text{CO}_2$  as a pure or concentrated stream, either through desorption of the  $\text{CO}_2$  under slight vacuum – which would require subsequent costly compression – or preferably, desorption into a sweep stream of pure  $\text{CO}_2$  at elevated pressure  $p^*$  (where  $p^* \gg p$ ). Such operation would be comprised of four main steps, as indicated in Figure 7a to d: (a)  $\text{CO}_2$  is taken up by reduced quinones until breakthrough; (b) air in the column is purged, displaced by pure  $\text{CO}_2$  at the desired product pressure  $p^*$ ; (c) quinones are oxidized to release  $\text{CO}_2$  into the pure gas sweep stream; (d) the pure  $\text{CO}_2$  in the column is displaced by the feed stream to be

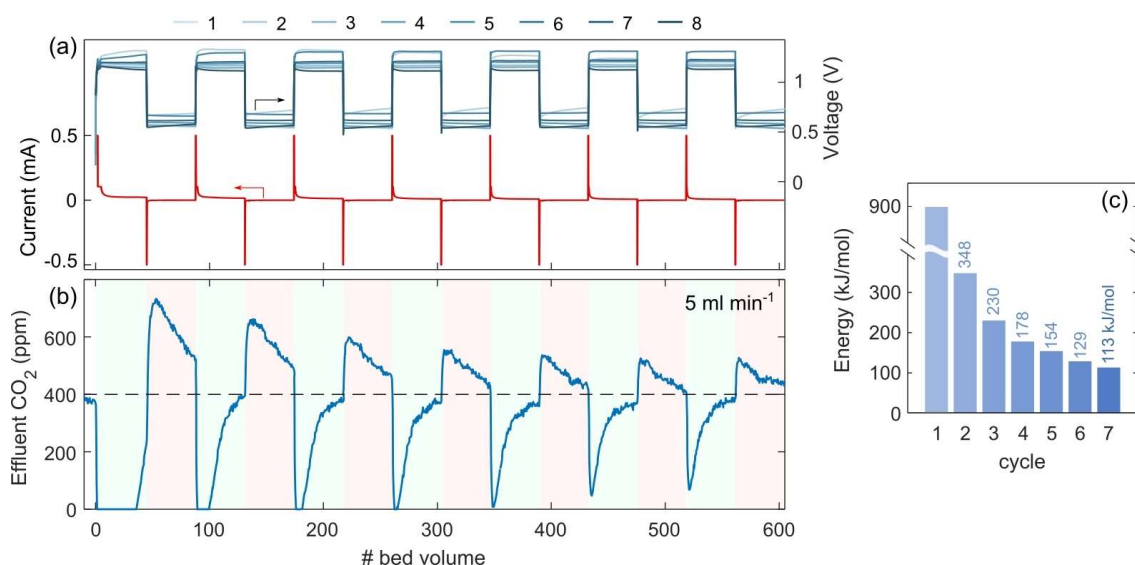


**Figure 6.** (a) Voltage of eight individual modules and the corresponding cell voltage as well as (b) effluent  $\text{CO}_2$  concentration for a multi-pair bipolar cell with 14 mL bed volume. Concentration profile reaches dynamic steady state with stable capture and release after 6–7 cycles. (c) Specific energy consumption (energy consumption per moles captured) for each cycle. Results show a clear tradeoff between capture rate and energy efficiency.

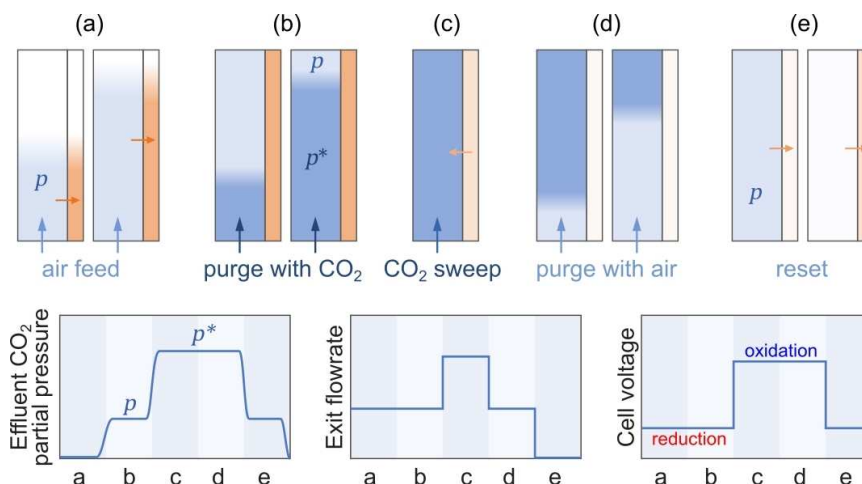


**Figure 7.** Schematic of an alternative swing process with capture from an air feed stream with  $\text{CO}_2$  partial pressure  $p$  and desorption into a sweep stream of pure  $\text{CO}_2$  at elevated pressure  $p^*$  (with  $p^* \gg p$ ). The corresponding effluent  $\text{CO}_2$  partial pressure, flowrate, and cell voltage during steps (a) to (e) is also shown.

treated; this displaced  $\text{CO}_2$  is part of the final product. Once the column has been filled with fresh air, the quinones are again reduced, and  $\text{CO}_2$  is adsorbed. Figure 7e indicates that the  $\text{CO}_2$  is adsorbed from the stagnant air filling the column before the next cycle is begun, but this step can be implicit in the first step of the next cycle. The nominal concentrations and flow rates of the effluent gas during the different stages are also shown.

The overall efficiency of the process relies on adsorption and desorption rates under different partial pressures, which highlights the importance of electrolyte selection, and specifically, the role of  $\text{CO}_2$  solubility in the electrolyte on the performance of the process. We here demonstrate the effect of  $\text{CO}_2$  solubility on both the working capacity and the transport dynamics. To this end, we consider the simple system shown in Figure 8, which captures many of the salient features of the

adsorption swing process. For simplicity, we assume a constant feed gas partial pressure  $p$ , quinone concentration  $c_Q$ , and interfacial concentration of the dissolved gas  $p/H$  (with  $H$  being the Henry's constant). The dissolved gas in the electrolyte diffuses into the electrode and reacts rapidly with quinone moieties at a reaction front that segregates the electrode into two regions: one with dissolved gas and fully-reacted quinones (with  $c_{Q,0}$  initial concentration). As the gas reaches the reaction front the quinone is consumed and the front moves further away from the interface. Under these conditions, with the quinone concentration significantly higher than the gas concentration, the reaction front moves sufficiently slowly that the pseudo-steady state assumption can be justified. The position of the reaction front  $\delta$  is obtained by equating the rate of quinone consumption to the flux of dissolved gas to the front. The defining equations are:

$$\frac{\partial^2 c}{\partial y^2} = 0 \quad \text{with} \quad \begin{cases} c = p/H \text{ at } y = 0 \\ c = 0 \text{ at } y = \delta \end{cases} \quad (2)$$

$$c_Q \frac{d\delta}{dt} = -D \left. \frac{\partial c}{\partial y} \right|_{y=\delta} \quad \text{with } \delta = 0 \text{ at } t = 0 \quad (3)$$

The solution to this set of equations is simply  $c = (p/H)(1 - y/\delta)$  and  $\delta = \sqrt{(p/Hc_Q)2Dt}$ . The molar flux of  $\text{CO}_2$  is thus  $j = (p/H)\sqrt{(c_Q H/p)(D/2t)}$ . Upon desorption, on the other hand, quinones release their full load of  $\text{CO}_2$  (i.e.,  $c_{Q,0}$ ), and the  $\text{CO}_2$  remaining in the electrolyte equilibrates at  $p^*/H$ , as the electrolyte equilibrates with the sweep stream with partial pressure  $p^*$  ( $p^* \gg p$ ). In the next cycle, this dissolved  $\text{CO}_2$  complexes fully with the reduced quinones such that the available quinone for uptake of the feed  $\text{CO}_2$  is now at concentration  $c_Q = c_{Q,0} - p^*/H$ , which is lower than the initial amount  $c_{Q,0}$ . The total capacity for  $\text{CO}_2$  adsorption is given by

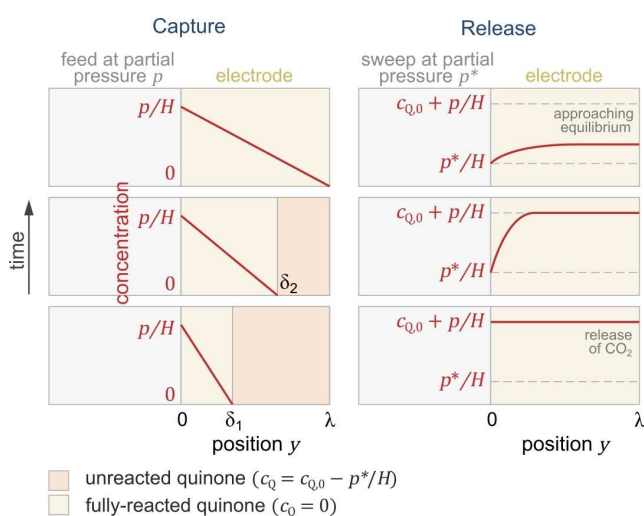


**Figure 8.** Schematic showing concentration profiles of dissolved  $\text{CO}_2$  based on a simplified quasi-steady state model during capture step (left) at partial pressure  $p$  and release step (right) at higher partial pressure  $p^*$ .



sum of the amount dissolved in the electrolyte and the amount that complexes with the available quinone, i.e.,

$$c_{\text{ads}} = \frac{p}{H} + \left( c_{\text{Q},0} - \frac{p^*}{H} \right) = \frac{p}{H} \left[ 1 + \left( \frac{c_{\text{Q},0}H}{p} - \frac{p^*}{p} \right) \right] \quad (4)$$

This is the maximum working capacity, which places a constraint on the quinone concentration required for a desired operation at partial pressures:  $c_{\text{Q},0} > (p^* - p)/H$ . This result clearly shows that, for a given partial pressure swing, electrolytes having a higher capacity for  $\text{CO}_2$  (lower  $H$ ) require higher quinone loading. Thus, from an overall utilization perspective, a lower solubility in the electrolyte is desired. On the other hand, low solubilities have an adverse effect on transport rates, as the flux during the subsequent capture step is now given by

$$j = \frac{p}{H} \sqrt{\left( \frac{c_{\text{Q},0}H}{p} - \frac{p^*}{p} \right) \frac{D}{2t}}$$

and the capture time (time to fully load the electrode of thickness  $\lambda$ ) is approximately  $t \approx \left( \frac{c_{\text{Q},0}H}{p} - \frac{p^*}{p} \right) \frac{\lambda^2}{2D}$ .

To gain insight into desorption dynamics, we consider the development of the  $\text{CO}_2$  concentration profile by assuming an initially uniform  $\text{CO}_2$  concentration of  $(c_{\text{Q},0} + p/H)$  and purely diffusive  $\text{CO}_2$  transport through the electrode towards the interface, which is at concentration of  $p^*/H$ . The first-order (long-time) solution can be written as:

$$c \approx \frac{p}{H} \left[ \frac{p^*}{p} + \left( \left( \frac{c_{\text{Q},0}H}{p} - \frac{p^*}{p} \right) + 1 \right) \frac{2}{\pi} \sin\left(\frac{\pi}{2\lambda}y\right) \exp\left(-\frac{\pi^2Dt}{4\lambda^2}\right) \right] \quad (5)$$

This solution, although simplified, indicates that for a given feed partial pressure  $p$ , with recovery into a sweep stream at  $p^*$ , the important parameters governing both the working capacity and the fluxes are  $(c_{\text{Q},0}H/p - p^*/p)$  and  $p^*/p$ , i.e., the quinone concentration (loading) relative to the  $\text{CO}_2$  concentration in the electrolyte at equilibrium and the ratio of the product partial pressure relative to that in the feed. Lastly, we note that while this derivation has been for an idealized system, and it has been assumed that equilibrium is reached in both the adsorption and desorption steps, the general conclusions regarding the impact of the governing parameters identified here can be expected to hold under more realistic operating conditions with smaller working capacities under non-equilibrium conditions.

## Conclusions

Carbon capture is crucial for mitigation of the unprecedented rise in the atmospheric concentration of anthropogenic  $\text{CO}_2$ . With the vast scale of distributed emission sources, this work focuses on direct air capture (DAC), as a viable solution for carbon removal. We demonstrated an electrochemically mediated DAC system with modular and expandable bipolar cell structure that utilizes redox activity of quinone moieties for effective capture and release of  $\text{CO}_2$ . Our electrochemical cell consisted of a series of PVAQ-CNT cathodes,

poly(vinylferrocene)-CNT (PVFc-CNT) anodes, 1-butyl-3-methylimidazolium bis(trifluoromethylsulfonyl)imide ([BMIM][TFSI]) ionic liquid electrolytes and separators (collectively, a module) that were electrically in-series. This led to a significant decrease in required volume for the system implementation, paving a way for potential application of the presented electrochemical technique at a large scale. Detailed investigation on the characteristics of the system depending on the operation voltage was carried out, which led to the successful demonstration of capture from (and release to) an extremely dilute stream of 400 ppm (0.04%)  $\text{CO}_2$  via a meso-scale eight-pair bipolar cell; specific energy consumption as low as 113 kJ per mole of  $\text{CO}_2$  at the optimized condition attests to the promise for electrochemically mediated DAC. We note that electrochemical techniques, unlike incumbent technologies that often require temperature and/or pH swings, rely entirely on simple voltage modulation, eliminating the need for use of chemical agents and addressing subsequent waste problems. Although a rigorous technoeconomic analysis and technological breakthroughs (such as addressing oxygen sensitivity of quinones and improving electrode architecture for enhanced uptake rates) are yet needed for actual applications, the abovementioned advantages of the electrochemical process presented in this study suggest that this technique is a promising option for mitigation of  $\text{CO}_2$ .

## Acknowledgements

This work was supported by Royal Dutch Shell. The authors greatly acknowledge Satoshi Morikawa and Dr. Hyowon Seo for their valuable assistance with initial investigation into the quinone polymer synthesis.

## Conflict of Interest

The authors declare no conflict of interest.

## Data Availability Statement

The data that support the findings of this study are available from the corresponding author upon reasonable request.

**Keywords:** bipolar stack · carbon dioxide capture · carbon storage · direct air capture · electrochemical separation

- [1] R. Alley, T. Berntsen, N. L. Bindoff, Z. Chen, A. Chidthaisong, P. Friedlingstein, J. Gregory, G. Hegerl, M. Heimann, B. Hewitson, B. Hoskins, F. Joos, J. Jouzel, V. Kattsov, U. Lohmann, M. Manning, T. Matsuno, M. Molina, N. Nicholls, J. Overpeck, D. Qin, G. Raga, V. Ramaswamy, J. Ren, M. Rusticucci, S. Solomon, R. Somerville, T. F. Stocker, P. Stott, R. J. Stouffer, P. Whetton, R. A. Wood, D. Wratt, J. Arblaster, G. Brasseur, J. H. Christensen, K. Denman, D. W. Fahey, P. Forster, E. Jansen, P. D. Jones, R. Knutti, H. Le Treut, P. Lemke, G. Meehl, P. Mote, D. Randall, D. A. Stone, K. E. Trenberth, J. Willebrand, F. Zwiers, *Climate Change 2007: The Physical Science Basis. Contribution of*

- Working Group I to the Fourth Assessment Report of the Intergovernmental Panel on Climate Change. Geneva, Switzerland, 2007. <https://www.ipcc.ch/report/ar4/wg1/> <https://www.ipcc.ch/site/assets/uploads/2018/02/ar4-wg1-spm-1.pdf>.
- [2] X. Shi, H. Xiao, H. Azarabadi, J. Song, X. Wu, X. Chen, K. S. Lackner, *Angew. Chem. Int. Ed.* **2020**, *59*, 6984–7006; *Angew. Chem.* **2020**, *132*, 7048–7072.
- [3] R. K. Pachauri, M. R. Allen, V. R. Barros, J. Broome, W. Cramer, R. Christ, J. A. Church, L. Clarke, Q. Dahe, P. Dasgupta, N. K. Dubash, O. Edenhofer, I. Elgizouli, C. B. Field, P. Forster, P. Friedlingstein, J. Fuglestad, L. Gomez-Echeverri, S. Hallegatte, G. Hegerl, M. Howden, K. Jiang, B. J. Cisneros, V. Kattsov, H. Lee, K. J. Mach, J. Marotzke, M. D. Mastrandrea, L. Meyer, J. Minx, Y. Mulugetta, K. O'Brien, M. Oppenheimer, J. J. Pereira, R. Pichs-Madruga, G.-K. Plattner, H.-O. Pörtner, S. B. Power, B. Preston, N. H. Ravindranath, A. Reisinger, K. Riahi, M. Rusticucci, R. Scholes, K. Seyboth, Y. Sokona, R. Stavins, T. F. Stocker, P. Tschakert, D. van Vuuren, J.-P. van Ypersele, R. K. Pachauri, L. A. Meyer, *Climate Change 2014: Synthesis Report. Contribution of Working Groups I, II, and III to the Fifth Assessment Report of the Intergovernmental Panel on Climate Change*. Geneva, Switzerland, 2014. <https://www.ipcc.ch/report/ar5/syr/> [https://www.ipcc.ch/site/assets/uploads/2018/02/SYR\\_AR5\\_FINAL\\_full.pdf](https://www.ipcc.ch/site/assets/uploads/2018/02/SYR_AR5_FINAL_full.pdf).
- [4] G. T. Rochelle, *Science* **2009**, *325*, 1652–1654.
- [5] F. L. Horn, M. Steinberg, *Fuel* **1982**, *61*, 415–422.
- [6] T. Harada, C. Halliday, A. Jamal, T. A. Hatton, *J. Mater. Chem. A* **2019**, *7*, 21827–21834.
- [7] C. Halliday, T. Harada, T. A. Hatton, *Ind. Eng. Chem. Res.* **2020**, *59*, 8937–8945.
- [8] Y. Liu, H. Z. Ye, K. M. Diederichsen, T. Van Voorhis, T. A. Hatton, *Nat. Commun.* **2020**, *11*, 2278.
- [9] M. Wang, M. Rahimi, A. Kumar, S. Hariharan, W. Choi, T. A. Hatton, *Appl. Energy* **2019**, *255*, 113879.
- [10] E. S. Sanz-Pérez, C. R. Murdock, S. A. Didas, C. W. Jones, *Chem. Rev.* **2016**, *116*, 11840–11876.
- [11] M. Fasihi, O. Efimova, C. Breyer, *J. Cleaner Prod.* **2019**, *224*, 957–980.
- [12] C. W. Jones, *Annu. Rev. Chem. Biomol. Eng.* **2011**, *2*, 31–52.
- [13] K. Lackner, H.-J. Ziock, P. Grimes, *Carbon Dioxide Extraction from Air: Is It an Option?* 24th Annual Technical Conference on Coal Utilization & Fuel Systems. Clearwater, Florida, 1999. <https://www.osti.gov/biblio/770509-carbon-dioxide-extraction-from-air-optionhttps://www.osti.gov/servlets/purl/770509>.
- [14] F. Zeman, *Environ. Sci. Technol.* **2007**, *41*, 7558–7563.
- [15] D. W. Keith, G. Holmes, D. St. Angelo, K. Heidel, *Joule* **2018**, *2*, 1573–1594.
- [16] V. Nikulshina, N. Ayesa, M. E. Gálvez, A. Steinfeld, *Chem. Eng. J.* **2008**, *140*, 62–70.
- [17] G. Hu, N. J. Nicholas, K. H. Smith, K. A. Mumford, S. E. Kentish, G. W. Stevens, *Int. J. Greenhouse Gas Control* **2016**, *53*, 28–40.
- [18] G. H. Rau, *Environ. Sci. Technol.* **2008**, *42*, 8935–8940.
- [19] C. Zhou, J. Ni, H. Chen, X. Guan, *Sustain. Energy Fuels* **2021**, *5*, 4355–4367.
- [20] L. A. Blanchard, D. Hancu, E. J. Beckman, J. F. Brennecke, *Nature* **1999**, *398*, 28–29.
- [21] Z. Xue, Z. Zhang, J. Han, Y. Chen, T. Mu, *Int. J. Greenhouse Gas Control* **2011**, *5*, 628–633.
- [22] G. Cui, J. Wang, S. Zhang, *Chem. Soc. Rev.* **2016**, *45*, 4307–4339.
- [23] S. Zeng, X. Zhang, L. Bai, X. Zhang, H. Wang, J. Wang, D. Bao, M. Li, X. Liu, S. Zhang, *Chem. Rev.* **2017**, *117*, 9625–9673.
- [24] X. Xu, C. Song, J. M. Andresen, B. G. Miller, A. W. Scaroni, *Energy Fuels* **2002**, *16*, 1463–1469.
- [25] W. R. Lee, S. Y. Hwang, D. W. Ryu, K. S. Lim, S. S. Han, D. Moon, J. Choi, C. S. Hong, *Energy Environ. Sci.* **2014**, *7*, 744–751.
- [26] T. Gelles, S. Lawson, A. A. Rownaghi, F. Rezaei, *Adsorption* **2020**, *26*, 5–50.
- [27] J. S. Kang, S. Kim, T. A. Hatton, *Curr. Opin. Green Sustain. Chem.* **2021**, *31*, 100504.
- [28] S. Jin, M. Wu, R. G. Gordon, M. J. Aziz, D. G. Kwabi, *Energy Environ. Sci.* **2020**, *13*, 3706–3722.
- [29] L. Legrand, O. Schaetzle, R. C. F. de Kler, H. V. M. Hamelers, *Environ. Sci. Technol.* **2018**, *52*, 9478–9485.
- [30] S. Zhu, J. Li, A. Toth, K. Landskron, *ACS Appl. Energy Mater.* **2019**, *2*, 7449–7456.
- [31] S. Voskian, T. A. Hatton, *Energy Environ. Sci.* **2019**, *12*, 3530–3547.
- [32] S. A. Didas, S. Choi, W. Chaikittisilp, C. W. Jones, *Acc. Chem. Res.* **2015**, *48*, 2680–2687.
- [33] P. Bollini, S. A. Didas, C. W. Jones, *J. Mater. Chem.* **2011**, *21*, 15100–15120.
- [34] D. G. Madden, H. S. Scott, A. Kumar, K.-J. Chen, R. Sanii, A. Bajpai, M. Lusi, T. Curtin, J. J. Perry, M. J. Zaworotko, *Philos. Trans. R. Soc. London Ser. A* **2017**, *375*, 20160025.
- [35] W. Choi, D. Harada, K. Oyaizu, H. Nishide, *J. Am. Chem. Soc.* **2011**, *133*, 19839–19843.
- [36] M. B. Mizen, M. S. Wrighton, *J. Electrochem. Soc.* **1989**, *136*, 941–946.
- [37] F. Simeon, M. C. Stern, K. M. Diederichsen, Y. Liu, H. J. Herzog, T. A. Hatton, *J. Phys. Chem. C* **2022**, *126*, 1389–1399.
- [38] I. Bahadur, K. Osman, C. Coquelet, P. Naidoo, D. Ramjugernath, *J. Phys. Chem. B* **2015**, *119*, 1503–1514.
- [39] A. Hemmatifar, J. W. Palko, M. Stadermann, J. G. Santiago, *Water Res.* **2016**, *104*, 303–311.
- [40] A. Ramachandran, A. Hemmatifar, S. A. Hawks, M. Stadermann, J. G. Santiago, *Water Res.* **2018**, *140*, 323–334.

---

Manuscript received: November 30, 2021

Revised manuscript received: January 17, 2022

Accepted manuscript online: January 21, 2022

Version of record online: February 15, 2022